Effects of Thermal-Carrier Heat Conduction upon the Carrier Transport and the Drain Current Characteristics of Submicron GaAs MESFETs

Jang Jyegal
(Department of Electronics Engineering, Junior College of Inchon)
제갈 장
(시립 인천전문대학 전자과)

Abstract

A 2-dimensional numerical analysis is presented for thermal-electron heat conduction effects upon the electron transport and the drain current-voltage characteristics of submicron GaAs MESFETs, based on the use of a nonstationary hydrodynamic transport model. It is shown that for submicron GaAs MESFETs, electron heat conduction effects are significant on their internal electronic properties and also drain current-voltage characteristics. Due to electron heat conduction effects, the electron energy is greatly one-dimensionalized over the entire device region. Also, the drain current decreases continuously with increasing thermal conductivity in the saturation region of large drain voltages above 1 V. However, the opposite trend is observed in the linear region of small drain voltages below 1 V. Accordingly, for a large thermal conductivity, negative differential resistance drain current characteristics are observed with a pronounced peak of current at the drain voltage of 1 V. On the contrary, for zero thermal conductivity, a Gunn oscillation characteristic is observed at drain voltages above 2 V under a zero gate bias condition.

I. Introduction

GaAs MESFETs are utilized as the key active device in high-frequency digital and analog integrated circuits, and their characteristic device dimensions are continuously decreasing with the ever-increasing demand of device operation in higher frequency ranges. The present progress in GaAs technology already results

in realizing production of commercial GaAs MESFETs with gate lengths of less than 0.3 μm.

In these small, high-electron-mobility devices, the transport of electrons under the gate is fully nonstationary due to a very short gate transit time comparable with their energy relaxation time, and also the electrons can be heated rapidly and significantly in the high-field channel region due to their high mobility and the development of a high electric field even at a moderate drain voltage. Hence, hot-carrier effects such as velocity overshoot and heat conduction can play an important role in carrier transport in the submicron devices.

A full hydrodynamic semiclassical model includes a heat flux term in the energy conservation equation to account for local spatial energy flows due to heat conduction by thermal carriers. However, since including the term greatly increases the numerical difficulty of finding a stable solution, heat conduction effects were neglected in the majority of two-dimensional submicron device simulations by assuming that the carrier distribution in k-space is simply a displaced Maxwellian[1, 2, 3-7]. It is demonstrated, however, that in GaAs, the distribution function of electrons is distorted significantly along the field direction even for an electric field of 10 kV/cm[8]. Generally, the assumption of a displaced Maxwellian distribution can be a poor approximation for the conduction band electrons of high-electron-mobility compound semiconductors.

Recently, several authors[9, 10, 11] have attempted to incorporate heat conduction effects into simulation using an analytic heat conductivity formulation based on the assumption of a simple power-law carrier scattering. However, this assumption is very invalid for GaAs because a power law does not exist for polar optical scattering and intervalley scattering, which are the dominant scattering processes in this material.

In the present paper, GaAs MESFETs with a gate length of 0.3 μm are simulated by using a full-energy-conservation hydrodynamic model to investigate thermal-electron heat conduction effects upon the carrier transport in submicron devices and also the drain current-voltage characteristics.

II. The Numerical Model

The numerical model used in the present work is based on semiclassical hydrodynamic equations which can be derived from the Boltzmann transport equation by the moment method. The model consists of a set of macroscopic conservation equations for particles, momentum and energy, respectively, as follows:

$$\frac{\partial n}{\partial t} + \nabla \cdot (n \mathbf{v}) = 0, \tag{1}$$

$$\mathbf{v} = -\frac{\tau_m(w)}{m^*(w)}\left[q\mathbf{E} + \frac{1}{n}\nabla(n k_B T)\right], \tag{2}$$

and

$$\frac{\partial w}{\partial t} + \mathbf{v} \cdot \nabla w = -q\mathbf{E} \cdot \mathbf{v} - \frac{1}{n}\nabla \cdot (n k_B T \mathbf{v}) + \frac{1}{n}\nabla \cdot (\kappa \nabla T) - \frac{w - w_o}{\tau_w(w)}, \tag{3}$$

where t is the time, q is the positive electronic charge, kB is the Boltzmann constant, E is the electric field, n is the electron concentration, v is the electron drift velocity, T is the electron temperature, κ is the thermal conductivity of the electron gas, and w is the average electron energy (wo is the thermal equilibrium value). The energy-dependent macroscopic parameters m*(w), τ m(w), and τ w(w) are the average effective mass and the momentum and energy relaxation times, respectively. These macroscopic transport parameters are assumed to locally depend only upon the average carrier energy, and their energy dependences can be accurately calculated by the ensemble Monte Carlo simulation under homogeneous electric field conditions.

The electron temperature T is described with the scalar electron drift velocity v by

$$T = \frac{2}{3 k_B}\left[w - \frac{1}{2} m^*(w) v^2\right], \tag{4}$$

and modeled by

$$\kappa = \Lambda(w) \left(\frac{k_B}{q} \right)^2 \sigma T(w), \tag{5}$$

where Λ(w) is the energy-dependent Lorenz number[12] and T(w) here is the stationary condition electron temperature.

The highly non-linear partial differential transport equations are solved numerically with connection with Poisson's equation. For a majority-carrier device, Poisson's equation can be written as

$$\nabla^2 \psi = -\frac{q}{\varepsilon_s} (N_d^+ - n), \tag{5}$$

where ψ is the electrostatic potential, N_d^+ is the ionized donor density, and ε s is the material dielectric permittivity. The electric field is evaluated from the solution of (5) by the electrostatic potential and field relationship.

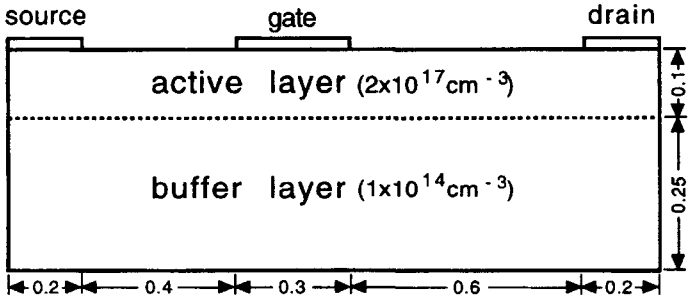

Fig. 1. Cross-section of the simulated submicron MESFET device, with dimensions in μm.

The device simulation for the analysis has been made for typical submicron GaAs MESFETs of 0.3 μm gate length at room temperature (300 K). The details of the simulated numerical device are schematically depicted in Fig. 1. As shown, the active layer thickness is 0.1 μm, and the buffer layer thickness is 0.25 μm, which is much thinner than those of the actual devices but is enough for the numerical study. The two layers have uniform doping densities of 2 x 1017 cm-3 and 1 x 1014 cm-3, respectively. The numerical method for spatial discretization is based on a 3-point finite difference scheme.

III. Numerical Analysis

Two sets of contour plots for comparison are presented through Figs. 2 and 3 for the distributions of the electrostatic potential, the average electron energy, and the electron concentration inside the simulated submicron device, in order to analyze thermal-electron heat conduction effects in submicron GaAs MESFETs. Both sets have been obtained for the same bias conditions of a drain voltage of 2 V and zero gate voltage ($Vd=2$ V *and* $V_g=0$ V). But the energy conservation conditions applied are different in (3). In Fig. 3, the heat conduction effects are included by using Monte Carlo calculated values of the Lorenz number, evaluated as a function of electron energy, for the thermal conductivity κ. However, for Fig. 4, the thermal conductivity κ has been assumed to equal zero in (3), and therefore the heat conduction effects are totally excluded in this figure.

In the figures, contour lines for potential and energy are plotted in steps of 0.2V and 0.05 eV, respectively, and those for concentration are plotted in steps of one tenth of the active layer doping density. The dotted line in each plot defines the boundary between the active layer and the buffer layer, which is located at a 0.1 μm depth from the top surface of the active layer.

Compared between Figs. 2 and 3, the potential distributions and the concentration distributions show not much difference on the whole, while the energy distributions show quite a great deal of difference between them, as can be easily visualized by referring to the surface plots of Fig. (4), corresponding to the contour plots Figs. 2(b) and 3(b). It is noted that by heat conduction effects the distribution of the average electron energy is surprisingly one-dimensionalized to a great degree over the entire region of the device. Major changes by heat conduction in the distribution of electron energy can be found in a buffer layer region under the drain, an active layer region between the gate and the drain, and also the Schottky depletion region under the gate.

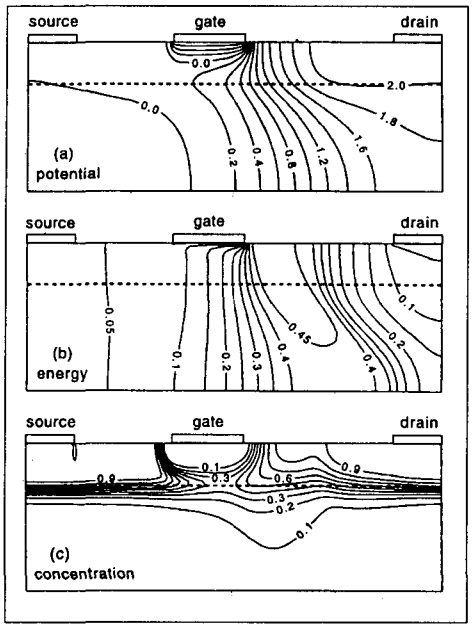

Fig. 2. Contour plots of the electrostatic potential (a), the average electron energy (b) and the electron concentration (c), including heat conduction effects.

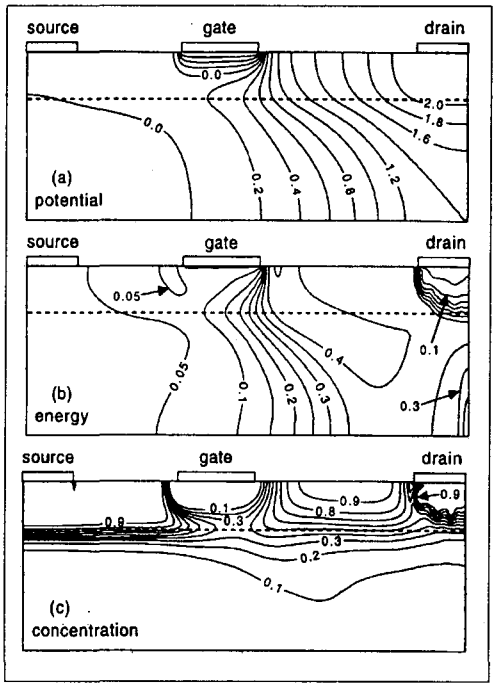

Fig. 3. As Fig. 2, but not including heat conduction effects.

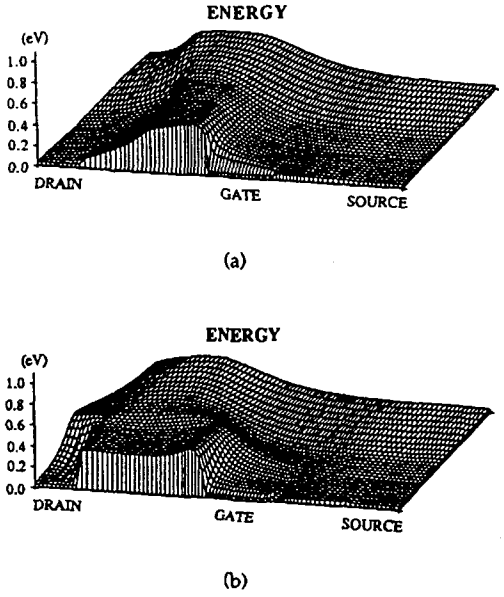

Fig. 4. Surface plots of the electron energy, including heat conduction effects (a) and not including heat conduction effects (b).

In the submicron devices, the local electric field between the gate and the drain can be very high because the applied drain voltage drops across the short gap between drain and gate electrodes. Therefore, the electron energy is very high throughout the entire region between the gate and the drain in Fig. 3(b), when no heat conduction is allowed. However, in Fig. 2(b), the energy is greatly reduced as a result of the heat conduction effect due to a possible large amount of heat flow into the neutral drain contact region of high carrier concentration and thermal equilibrium, since the neutral drain contact region acts as an efficient sink of the thermal energy of carriers. The electron energy therefore continuously decreases with a large slope by thermal-electron heat flows from the high-energy region near the gate toward the neutral drain contact region in Fig. 2(b).

In Fig. 2(b) or Fig. 4(a), there exists a large local thermal energy gradient in the active layer region between the gate and the drain. Therefore, since the electric field and the thermal energy gradient contribute to the electron velocity in

the same direction, the local electric field is reduced and hence the electrons are not depleted in the most part of the active layer between the gate and the drain in order to satisfy the current continuity equation. It is seen that the distributions of the electron concentration and the potential are thereby also significantly changed in the corresponding region in Fig. 2. The heat conduction effect is found to hardly allow the active layer to become depleted widely toward the drain region by the drain electric field, causing the applied drain voltage to mostly drop in the gate region. This eventually results in the formation of a much more stronger stationary high-field dipole domain well confined in a narrower region near the gate, and thereby the reaching of a higher maximum energy of electrons in the gate region (compare Figs. 2 and 3).

There is a large spatial variation in electron concentration across the junction between the active layer and the buffer layer so that the energy transport is mainly governed by the heat conduction term. In such a case, the energy of electrons is spatially conserved effectively by reducing their thermal energy gradient across the junction, which results in the significantly large change of energy distribution over the buffer layer region under the drain.

In the Schottky depletion region, there is a large gradient of thermal energy density, from the high-energy region toward the Schottky depletion region. Therefore, by some heat flows from the high-energy region under the drain side of the gate, the electron energy in this depletion region is also noted to be raised considerably in Fig. 2(b).

In Fig. 5, three different sets of full drain current-voltage characteristics obtained for the 0.3 μm gate-length device with different thermal conductivity conditions are presented and compared for thermal-electron heat conduction effects upon the drain current characteristics of submicron GaAs MESFETs. The different three thermal conductivity conditions are Λ=0, Λ=2.5, and Λ(w)=Monte Carlo calculated values, denoted by M.C in the figure, in (5).

It is observed that in the saturation region of large drain voltages above Vd=1 V, the drain current continuously decreases with increasing thermal conductivity.

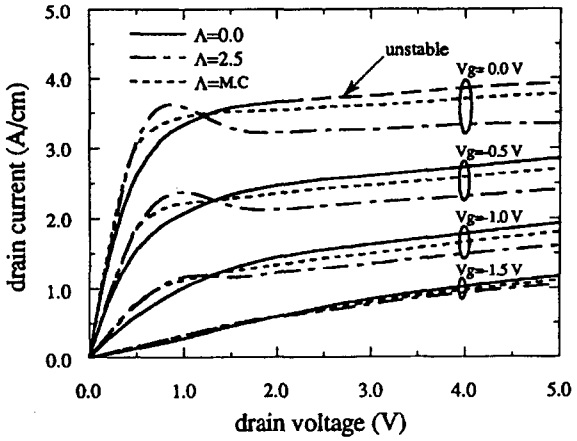

Fig. 5. Effects of thermal electron heat conduction upon the drain current-voltage characteristics.

The drain current difference between the two cases of Λ=0 and Λ=2.5 is large. However, in the linear region of small drain voltages below Vd=1 V, the opposite trend is observed and the drain current increases with increasing thermal conductivity. In particular, as the thermal conductivity becomes large (Λ=2.5), negative differential resistance (NDR) characteristics appear with the drain current reaching a pronounced peak point at Vd=1 V and then dropping back toward a dip at a larger drain voltage. Such NDR characteristics are usually not observed experimentally for real devices, but only observed numerically for short-channel devices when simulations are made using local stationary drift-diffusion models. Simulations based on nonstationary hydrodynamic models do not show NDR characteristics.

In addition, it is also important to note that when the thermal conductivity is totally neglected (Λ=0), a Gunn oscillation characteristic appears at drain voltages above 2V at zero gate voltage. The drain current becomes unstable by the Gunn oscillation at these bias conditions. In the figure, pentode-like drain current characteristics are observed for an accurate thermal conductivity based on the use of the Lorenz number evaluated by Monte Carlo calculation.

IV. Conclusion

Thermal-electron heat conduction effects in submicron gate-length *GaAs* MESFETs have been investigated and analyzed by a 2-dimensional numerical simulation using a hydrodynamic transport model. A typical device of 0.3 μm gate length has been used for the numerical simulation.

It has been found that electron heat conduction effects are significant on the distributions of the potential, the electron concentration, and the electron energy inside the submicron devices. In particular, it has been shown that the distribution of the electron energy is affected greatly, so that the 2-dimensional nature of energy distribution changes to an almost one-dimensional one. This one-dimensionalization in the energy distribution results in the large changes of the potential and the carrier concentration distribution in the active layer between the gate and the drain.

Also, it has been shown that in the saturation region of large drain voltages above Vd=1 V, the drain current continuously decreases with increasing thermal conductivity. However, in the linear region of small drain voltages below Vd=1 V, the opposite trend is observed. Thus, for a large thermal conductivity, the usual pentode-like drain current characteristics change to NDR characteristics with pronounced peaks of drain current at Vd=1 V. On the contrary, for zero thermal conductivity, a Gunn oscillation characteristic is observed at drain voltages above $2V$ at zero gate voltage.

References

[1] C. M. Snowden and D. Loret, "Two-dimensional hot-electron models for short-gate-length GaAs MESFET's," IEEE Trans. Electron. Devices, vol. ED-34, no. 2, pp. 212-223, 1987.

[2] Y. Feng and A. Hintz, "Simulation of submicrometer GaAs MESFET's using

a full dynamic transport model," IEEE Trans. Electron. Devices, vol. ED-35, no. 9, pp. 1419-1431, 1988.

[3] S. El-Ghazaly and T. Itoh, "Inverted-gate field-effect transistor: novel high-frequency structures," IEEE Trans. Electron Devices, vol. ED-35, no. 7, pp. 810-817, 1988.

[4] F. Heliodore, M. Lefebvre, G. Salmer, and O. L. El-Sayed, "Two-dimensional simulation of submicrometer GaAs MESFET's: surface effects and optimization of recessed gate structures," IEEE Trans. Electron Devices, vol. ED-35, no. 7, pp. 824-830, 1988.

[5] S. El-Ghazaly and T. Itoh, "Two-dimensional numerical simulation of short-gate-length GaAs MESFETs and application to the travelling Gunn domain phenomenon," Int. J. Numerical Modelling, vol. 1, pp. 19-30, 1988.

[6] T. Shawki, G. Salmer, and O. El-Sayed, "MODFET 2-D hydrodynamic energy modeling: optimization of subquarter-micron-gate structures," IEEE Trans. Electron Devices, vol. ED-37, no. 1, pp. 21-30, 1990.

[7] R. K. Cook and J. Frey, "Diffusion effects and ballistic transport," IEEE Trans. Electron Devices, vol. ED-28, no. 8, pp. 951-953, 1981.

[8] W. Fawcett, A. D. Boardman, and S. Swain, "Monte Carlo determination of electron transport properties in gallium arsenide," J. Phys. Chem. Solids, vol. 31, pp. 1963-1990, 1970.

[9] D. Widiger, K. Hess, and J. J. Coleman, "Two-dimensional numerical analysis of the high electron mobility transistor," IEEE Electron Device Lett., vol. 5, no. 2, pp. 266-269, 1984.

[10] G. Baccarani and M. R. Wordeman, "An investigation of steady-state velocity overshoot in silicon," Solid-St. Electron., vol. 28, no. 4, pp. 407-416, 1985.

[11] T. Wang and C. Hsieh, "Numerical analysis of nonequilibrium electron transport in AlGaAs/InGaAs/GaAs pseudomorphic MODFET's," IEEE Trans. Electron Devices, vol. ED-37, no. 9, pp. 1930-1938, 1990.

[12] Jang Jyegal, "2-D simulation of submicron GaAs MESFETs including thermal carrier heat conduction effects," J. Junior College of Inchon, vol. 25, pp. 171-185, 1996.